Materials & Design 268 (2026) 116509

Contents lists available at ScienceDirect

Materials & Design

journal homepage: www.elsevier.com/locate/matdes

Additive manufacturing of patient–specific lattice prosthetic sockets via field–driven design and elastic–plastic homogenization

P. Borracci [a,1], D. Menel [b,1], L. Romanelli [b,1], R. De Biasi [b,d], F. Napoleoni [a], I. Senegaglia [c], P. Neri [c], C. Santus [c], M. Controzzi [a,*], M. Benedetti [b,*]

[a] The Biorobotics Institute, Scuola Superiore Sant'Anna, Pontedera, PI 56025, Italy
[b] Department of Industrial Engineering, University of Trento, Trento 38123, Italy
[c] Department of Civil and Industrial Engineering, University of Pisa, Pisa 56122, Italy
[d] Department of Chemical Engineering Materials Environment, Sapienza University, Roma 00185, Italy

ARTICLE INFO

Keywords:
Prosthesis
Human-centred design
Lattice structure
Elastic-plastic homogenization
Lightweight field-driven design
Additive manufacturing

ABSTRACT

The development of patient-specific prosthetic sockets requires the integration of clinical data with advanced design methodologies to ensure both comfort and mechanical reliability. In this work, we propose a digital workflow combining 3D scanning of the residual limb, anatomical reconstruction, and computational design. The approach integrates elastic–plastic homogenization with a Field-Driven Design (FDD) strategy, where stress fields obtained from finite element analysis are mapped to spatially varying lattice properties and geometries. This approach enables a direct stress-to-structure transition for the design of lightweight, graded lattice sockets. The methodology is applied to a personalized socket manufactured via Multi Jet Fusion in PA12. Numerical simulations and experimental testing of a full-scale prototype demonstrate a weight reduction of up to 25% compared to a solid design, while maintaining a robust safety factor. Computed tomography analysis confirms good agreement between the as designed and as-built geometries. The proposed framework highlights the potential of integrating clinical data and Field-Driven lattice Design for next-generation and personalized prosthetic devices.

1. Introduction

Upper limb amputees rely on prosthetic devices to restore essential motor functions. Due to the high variability in residual limb anatomy and functional requirements, these devices must be highly personalized to ensure comfort, usability, and long-term acceptance. Within the prosthetic system, as illustrated in Fig. 1, the suspension system plays a central role as the interface between the user and the device.

The inner socket is the internal prosthetic interface in direct contact with the residual limb. Its main functions are to provide comfort, distribute pressure evenly, improve suspension, protect soft tissues during daily use, and accommodate the integration of EMG electrodes. The outer socket, instead, is the external structural component of the prosthesis responsible for mechanical support and load transfer during daily activities. It houses and stabilizes the inner socket while also enabling the integration of additional functional elements, such as attachment systems or electronic components, making it essential for both comfort and structural performance.

Traditional manufacturing methods are time-consuming and completely rely on the prosthetist's manual expertise [1–4]. Moreover, the user must be physically present for repeated fitting sessions, which can be burdensome and inefficient.

In this context, Additive Manufacturing (AM) offers an alternative pathway toward more efficient, reproducible, and innovative prosthetic solutions [5,6]. Integrating 3D scanning with digital modeling can improve the precision of customization while significantly reducing production time and effort. AM also enables the design of advanced geometries, including lattice structures, which can reduce the weight of prosthetic components without compromising mechanical integrity [7]. Minimizing weight is essential, as overly heavy devices often lead to discomfort and are a primary reason for user abandonment. Commercial examples are already exploring the benefits of the additive manufacturing [7–9].

However, despite the potential of AM to revolutionize prosthetic socket fabrication, challenges remain. These include the need for process standardization, validation of mechanical reliability, and regulatory

* Corresponding authors.
E-mail addresses: marco.controzzi@santannapisa.it (M. Controzzi), matteo.benedetti@unitn.it (M. Benedetti).
[1] Equally contributed to the manuscript.

https://doi.org/10.1016/j.matdes.2026.116509
Received 8 April 2026; Received in revised form 5 June 2026; Accepted 24 June 2026
Available online 2 July 2026
0264-1275/© 2026 The Author(s). Published by Elsevier Ltd. This is an open access article under the CC BY-NC-ND license (http://creativecommons.org/licenses/by-nc-nd/4.0/).

compliance for 3D-printed medical devices. Ensuring safety, functionality, and durability is thus critical before widespread clinical adoption can be realized [10,11]. A promising approach to address these challenges involves lattice structures, a subset of architected cellular materials [12]. Lattice structures are classified into three types: strut-based, plate-based and triply periodic minimal surface (TPMS)-based. These structures provide high stiffness-to-weight ratios, tunable mechanical properties, and geometric adaptability to complex anatomical shapes, as required in advanced biomedical applications [13].

In particular, strut-based lattice cells demonstrate exceptional capabilities in load distribution and energy dissipation; however, they exhibit susceptibility to manufacturing defects and structural instability, especially under compressive loading conditions [14]. On the contrary, TPMS-based designs incorporate continuous surface structures that offer greater stiffness and better resistance to local deformation [15]. However, their elaborate geometry and uninterrupted surface elements make it challenging to model their mechanical response accurately, especially when nonlinear effects are present [16]. Finally, plate-based lattices are also gaining attention given that they own exceptional structural rigidity, which qualifies them as particularly suitable for load-transfer and weight-supporting applications [17,18]. In addition, they can be efficiently applied to curved surfaces for applications that require structural shell behaviour. The mechanical properties of lattice structures depend on four main factors: the morphology of the unit cell, its tessellation, the relative density and the bulk material properties, and these latter characteristics can be manipulated to achieve desirable configurations and mechanical properties as documented in [19]. Besides this, recent advances in AM enabled the design and manufacturing of novel bio-inspired lattice structures with enhanced function properties as in [20] where closed-cell lattices, bio-inspired by sea urchin and fabricated from hyperplastic polymers, exhibited superior energy absorption when designed with thin walls rather than thick walls while maintaining the same relative density. Complementing this, atomic-level biomimicry has enabled advanced functional architecture materials (AFAMs), which leverage edge-to-edge tessellation inspired by cubic metallic crystals (SC, BCC, FCC) [21]. Unlike conventional lattices with uniform topology, AFAMs allow multiple unit cell types to be strategically interlocked, each exhibiting distinct mechanical behaviour. This enables spatially programmable properties and multi-material performance beyond traditional functionally graded structures.

Nonetheless, simulating the mechanical behaviour of such detailed architectures poses computational challenges. Finite Element Method (FEM) models of full lattice geometries are computationally intensive and often impractical for full-scale designs. To overcome this, homogenization methods have been employed. Originally developed for composite materials [22,23], homogenization involves replacing the complex geometry of the lattice with a fictitious continuum possessing equivalent macroscopic mechanical properties. These properties are derived from a Representative Volume Element (RVE) that characterizes the response of the lattice unit cell under various loading conditions. Elastic-plastic homogenization techniques further enable modelling of non-linear behaviour, thereby enhancing predictive accuracy in critical load-bearing applications [24–26,26–32].

Given the complexity of designing prosthetic sockets, computational design approaches can help systematically address both functional and user-driven requirements [33,34]. Field-Driven Design (FDD) is a particularly promising methodology in this context [35]. FDD uses scalar or vector fields, such as stress or density distributions, to guide local geometric modifications. In our work, field values are mapped directly onto the lattice infill percentage, reinforcing high-stress regions and reducing density in less stressed areas. Unlike topology optimization, which removes material through iterative procedures, FDD provides smooth transitions and continuous control over material distribution by directly mapping field values onto parameters such as wall thickness or lattice strut diameter, without relying on computationally expensive iterative solvers [35,36]. In biomedical engineering, FDD has been used to develop devices with regions of varying stiffness, porosity, or strength aligned with physiological demands. Applications include porous maxillofacial plates [37] and limb prostheses designed for stress shielding reduction and osseointegration [38,39]. These examples demonstrate how FDD can bridge the gap between mechanical optimization and biological compatibility. More recently, data-driven approaches combining computational simulation and machine learning have also been explored for predicting functional properties in additively manufactured lattice structures, such as transport and permeability behaviour [40].

The present study builds on these insights by proposing a novel holistic digital workflow for designing and validating a personalized, lightweight prosthetic socket. For the first time, we combined 3D scanning of the amputee stump, digital design incorporating lattice structures optimized using elastic–plastic homogenization and Field-Driven assignment of strut diameters in a comprehensive design pipeline. Validation was achieved through finite element simulations, experimental tensile testing of representative specimens and a quasi-static experimental test of the designed prosthetic device.

The following section provides a detailed description of the traditional method for the design and manufacturing process of upper limb prosthetic devices followed by a state of the art of the innovative technique for digital and non-contact design in the prosthetic field.

1.1. Traditional method

The traditional method for socket fabrication, depicted in Fig. 2 involves a series of manual steps, often time-consuming, carried out by the orthopaedic technician, who is the only professional qualified to modify the socket during the device construction process [41]. This method also requires the physical presence of the amputee at multiple stages to allow for continuous adjustments and verification.

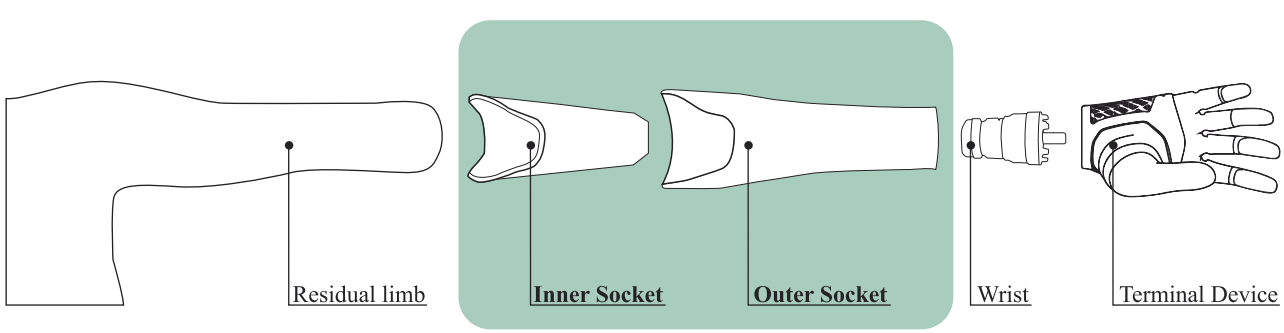

Fig. 1. Components of a typical prosthesis for a transradial amputee. The prosthesis is anchored to the amputee's residual limb by means of the suspension system, which consists of the inner socket and outer socket. Electromyography (EMG) electrodes, electronics and the battery are not represented: these components are in general housed in the socket.

Fig. 2. Traditional fabrication process of inner and outer prosthetic sockets. The procedure involves creating a negative mold of the residual limb in plaster, producing a transparent resin prototype for initial fitting, and refining the geometry through heating adjustments. Once the definitive positive mold is obtained, the inner socket is manufactured (typically using silicone-impregnated gauze) followed by the lamination of the outer socket with composite materials such as carbon or glass fibers and resin.

Initially, a mold of the residual limb is created using materials such as plaster, to accurately replicate the shape and dimensions of the patient's stump. This negative mold is then used to produce a transparent resin prototype, which serves as a first trial version of the inner socket. The prototype is tested directly on the amputee and adjusted using a heat source to enhance its fit and comfort. Once satisfactory adherence to the stump is achieved, a second plaster casting is performed to obtain the definitive positive model. The final inner socket is then fabricated on this positive mold, typically using silicone-impregnated gauze. Subsequently, the outer socket is constructed by moulding it directly over the inner socket. In this phase, composite materials such as resin and carbon or glass fibers are used, selected for their strength and lightness. The length and anatomical shape of the socket are defined in collaboration with the amputee and based on their individual anthropometry [42]. These multiple steps and repeated in-person appointments place a considerable time burden on the patient and, if present, their caregiver, particularly for those with limited mobility or logistical constraints.

1.2. State of the art of digital design

In recent years, prosthetic design has evolved toward more personalized and digitally driven methods, incorporating tools such as 3D scanning, CAD/CAM, finite element analysis (FEA), and additive manufacturing to optimize comfort, fit, and safety [43–47] CAD/CAM systems have enabled diverse clinical models—from in-house to centralized external fabrication-with improvements in cost-effectiveness, efficiency, and reproducibility [48,49]. For instance, the Virtual Socket Laboratory replicates traditional socket-shaping techniques using a digital interface enriched with domain knowledge to guide technicians during design [48]. In parallel, new computational frameworks integrate non-invasive imaging like MRI with patient-specific simulations and 3D printing to reduce manual trial-and-error iterations [44,50]. Materials used in prosthetic liners have also seen substantial innovation: Yang et al. [51] reviewed the advantages of elastomeric materials (e.g., silicone, thermoplastic elastomers, polyurethane) that can be tailored in thickness and stiffness to patient anatomy, for example improving pressure distribution and comfort as in [52]. Despite technical progress, however, many of these systems remain largely focused on fabrication aspects. They often neglect a full consideration of user-centred needs, such as long-term usability, lightweight, and psychosocial aspects, which are crucial to real-world prosthetic acceptance [49,53,54].

1.3. A multidisciplinary design approach

Designing prosthetic sockets extends beyond mechanical performance, as they must interface directly with the user's residual limb while meeting stringent ergonomic and physiological requirements. An effective socket should be lightweight, breathable, comfortable, and easy to don and doff, while also allowing natural movement of the proximal articulations and accommodating the integration of electronic components. Achieving this balance requires a multidisciplinary approach that combines engineering precision with human-centred design principles.

A systematic review by Borracci et al. [55] identified and prioritized over 600 user-reported needs concerning upper limb prostheses. Considering the suspension system, robustness emerged as the highest priority (11.7%), followed by affordability (9.8%), ergonomics (6.9%), and lightweight design (4.1%). In contrast, aspects such as thermal comfort and ease of donning were ranked lower, suggesting that these concerns may have been perceived as secondary to functional requirements or at least partially addressed in previous designs. To translate these qualitative insights into actionable design criteria, a House of Quality (HoQ) framework was employed (see Appendix A). The

HoQ is particularly useful in this context as it systematically maps user priorities to technical specifications, enabling a transparent assessment of how design decisions contribute to perceived value. This analysis highlighted the critical role of the socket material(s) (100% relevance), ingress protection against dust (82.1%), and impact resistance (65.8%) in meeting user expectations and performance targets. These findings are consistent with existing literature, which emphasizes the influence of material properties on durability and user comfort, as well as the importance of environmental protection and mechanical robustness for long-term prosthesis reliability in daily living conditions. The ergonomic and comfort analysis is not definitive but represents a preliminary assessment that has not yet been experimentally validated.

2. Materials and methods

The design process of a tailored upper limb prosthesis follows different steps concerning patient comfort, restoration of the functionality of the missing limb, statical, manufacturing and esthetical concerns. As mentioned, the process is multidisciplinary and complex, and a proper design tool such as the HoQ is of paramount importance in the initial design stage [55]. Building on this analysis of the requirements, the work proposes a design workflow and its experimental validation for an upper limb prosthetic device. The research effort was focused on the definition of a viable digital method able to acquire the anatomical dimensions of the amputee and the implementation of a custom lattice-based lightweight geometry for the socket. To achieve a lightweight design, we conducted computationally efficient numerical simulations on the designed socket, combined them with an innovative stress-driven optimization approach. The resulting device was manufactured and experimentally validated to prove the design soundness.

2.1. A new digital design pipeline

Starting from the requirements defined in the previous study [55], the design of the socket was carried out considering both technical constraints (e.g., load resistance up to 100 N, component integration, and dimensional limits) and user needs (comfort, stability, breathability, aesthetics). For this purpose, a volunteer amputee recruited through Orthopedic Panini in Milan (Italy) underwent 3D scans of the stump, contralateral limb, and plaster model. The scanning program used was Ortenshape (v2024, PROTEOR, USA) using the camera of an iPhone 15 Pro Max, while Meshmixer (v2024, Autodesk, USA), Fusion 360 (v2024, Autodesk, USA) and nTop (v2024, nTopology Inc., USA) software were used to manipulate the output geometry. Prior to participation, the amputee provided written informed consent in accordance with the EU Regulation 2016/679 on the protection of natural persons concerning the processing of personal data (General Data Protection Regulation – GDPR), and with the Italian Legislative Decree no. 196 of 30 June 2003, as amended by Legislative Decree no. 101 of 10 August 2018. This study was approved by the local ethical committee of the Scuola Superiore Sant'Anna, Pisa, Italy (approval n. 21/2022).

The design procedure of the inner socket is shown in Fig. 3: Starting from the plaster scan, the liner was generated by offsetting and trimming surfaces along anatomical landmarks. An initial prototype was fabricated and tested by the user, revealing anterior regions that required adjustment. Two iterations were sufficient to correct the global alignment of the liner, while additional two were performed to refine local geometry in the anterior area. Through this iterative process, a final liner was obtained, tailored to the user's anatomy and optimized for suspension and comfort. In parallel, as outlined in Fig. 4, the outer socket was developed to both restore anatomical proportions and house the functional components of a myoelectric hand prosthesis (batteries, electronics, dry electrodes, and wrist). Using the aligned scans as a reference, the socket geometry was shaped to conform to the liner up to a specified length, beyond which it transitioned into the section accommodating the wrist and embedded electronics.

Throughout the design, attention was paid to minimizing bulk parts, improving component accessibility, and preserving anatomical coherence. For instance, we leveraged the design freedom guaranteed by additive manufacturing and we integrated the battery compartment and wrist housing into a single part. This acts as a plug-in structure and is fixed to the socket via a radial bolted flange. This solution allows for straightforward insertion and removal during assembly and maintenance, reducing the number of parts and simplifying integration with

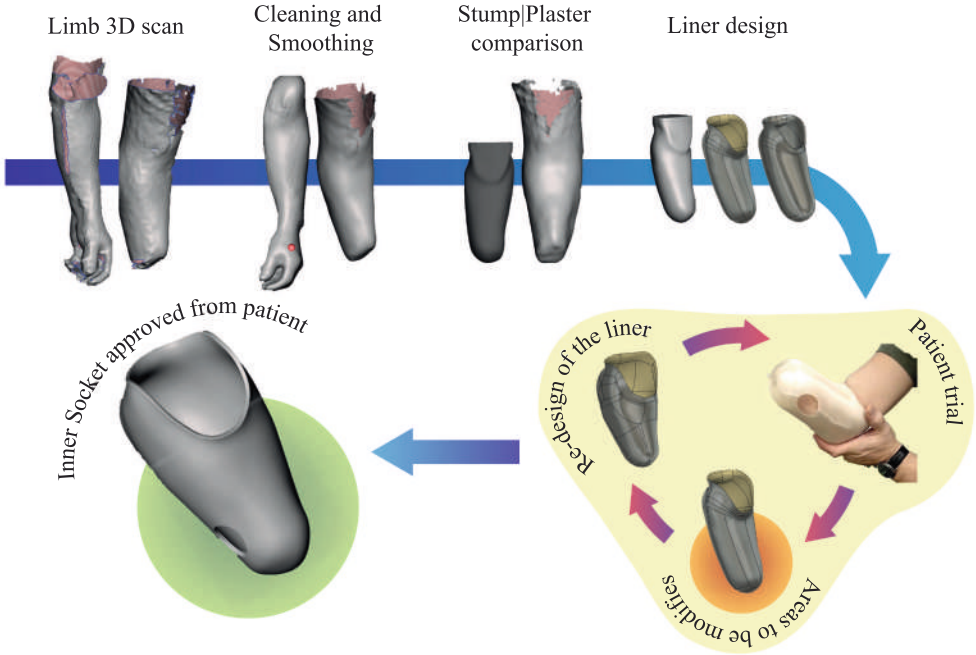

Fig. 3. Inner socket design procedure. Starting from the plaster scan using Ortenshape, the liner geometry was generated by offsetting and trimming along anatomical landmarks using Fusion 360. A first prototype was fabricated with 3D printing and tested by the user, highlighting anterior regions requiring adjustment. Through successive redesign and fitting iterations, a final liner was achieved, optimized for anatomical fit, suspension, and comfort.

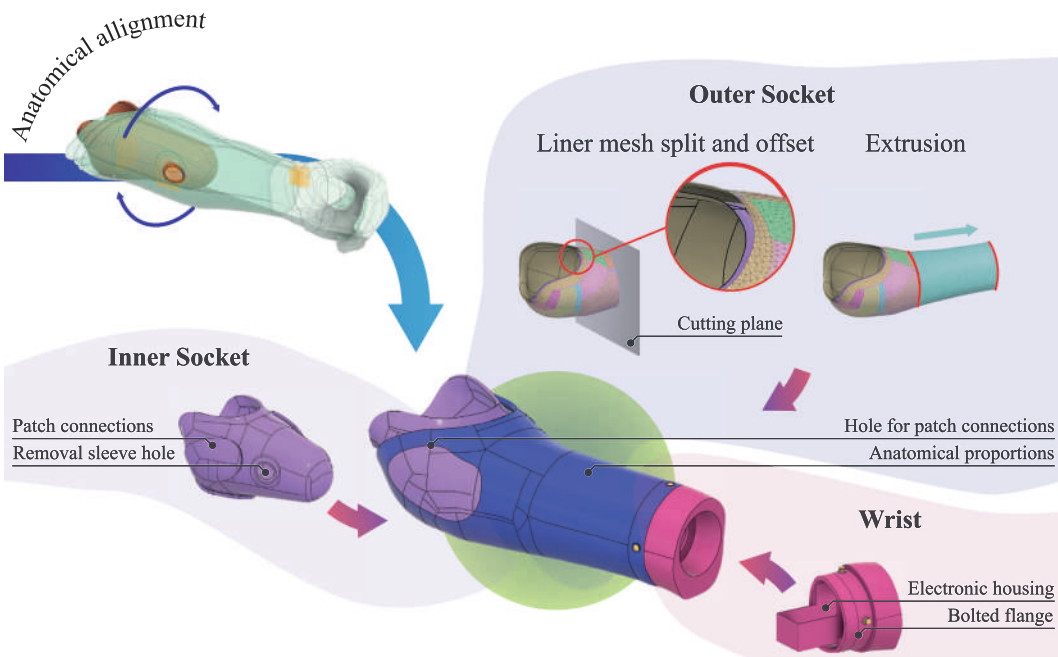

Fig. 4. Outer socket design procedure using Fusion 360. The geometry was developed to restore anatomical proportions while accommodating the functional components of a myoelectric prosthesis, including batteries (e.g. model: 704,878 by ACCU ITALIA® spa), electronics, dry electrodes (e.g. model: 13E200 = 50 by Ottobock®), power unit (designed and supplied by Prensilia S.r.l.) and wrist (e.g. Quick Disconnect Wrist by Ottobock®). Using aligned scans as a reference, the outer shell was shaped to conform to the liner up to a defined length, then transitioned into the distal section housing the wrist and embedded electronics.

the hand system. The design choice to directly connect the liner and socket components by solid patches, without relying on traditional riveting, follows the same idea.

Multi-Jet Fusion (MJF) was selected as manufacturing technique for its excellent characteristics in terms of geometrical accuracy, resolution and productivity [56]. Specifically, an HP Jet Fusion 4200 printer was employed. The selected material is HP 3D reusability PA12 (provided by HP, USA), characterized by a competitive trade-off between mechanical properties, biocompatibility, printability and cost [57].

2.2. Lattice structure design and modelling technique

A single-layer lattice shell was adopted for the structural design of the socket, primarily due to its compatibility with the anatomy-inspired geometry of the outer shell. A 2D lattice was applied conformal to the socket shape and lattice RVE was composed by the superposition of diagonal and square lattice geometry. This cell topology provided robust, hyperstatic and almost isotropic behaviour, well suited for complex shapes. The application of this lattice pattern to the socket geometry was performed by applying the lattice on the component surface mesh. This procedure generated limited and localized distortions of the lattice pattern. These effects are considered negligible in the global behaviour of the prosthetic.

To inform the design process and enable efficient parameterization, a computational homogenization analysis was performed on the selected lattice unit cell. While linear elasticity is often assumed for simplicity, the material used (PA12) exhibits non-negligible plasticity under load conditions relevant to the socket use, especially at thin cross-sections. Therefore, an elastic–plastic homogenization approach was employed to better capture the effective mechanical response of the lattice under physiological stresses. This allowed us to quantify the equivalent stiffness and yield strength of the lattice material, thereby supporting informed decisions on wall thickness, unit cell dimensions, and load-bearing capacity within the design envelope of the prosthetic device. The resulting homogenized properties were then used to parameterize the graded lattice architecture within the prosthetic socket. The full mathematical formulation of the homogenization procedure, including derivations of the governing equations, parameter identification, and details of the finite element implementation, is coherent with [58] and reported in Appendix B. The input elastic mechanical properties of PA12 bulk material were $E_b = 1120$ MPa and $\nu_b = 0.40$ as in [58], while the input plastic curve was introduced in the FE model as a lookup table and the reader can address it in the appendix of [58]. In addition, "HP 3D High Reusability PA 12" powder, supplied by HP, was used during the manufacturing. According to [59] the main properties of the powder, such as powder melting point, average particle size and bulk density of powder, were equal to 187 °C, 60 μm and 0.425 g/cm^3, respectively.

The homogenization process was applied to a predefined set of ten strut diameters ranging from 0.5 to 5 mm. The upper bound was chosen to reflect the thickness of the socket's outer walls (4.0–5.5 mm) while the lower bound was constrained by manufacturing limitations. The minimum strut dimension was subsequently increased in the design: very thin struts would create excessive differences in thickness across the structure, leading to local compliance, reduced overall stiffness, and higher sensitivity to defects. Thus, the minimum diameter was set at 1.5 mm to achieve a more uniform and mechanically reliable lattice architecture, balancing lightweighting with defect tolerance.

2.3. Field-driven numerical simulation workflow

This section presents a Field Driven Design (FDD) approach aimed at optimizing the lattice density based on local stress conditions, enabling efficient material distribution and performance tuning. The core principle of this method is the correlation between stress magnitude and lattice strut diameter: regions subjected to higher mechanical demand are reinforced with thicker struts, whereas low-stress areas are lightened using thinner elements.

To perform the FDD, a complete Finite Element (FE) analysis on the socket was performed, as depicted in Fig. 5. A loading condition resembling the socket use scenario was selected: a fixed support was applied at the inner liner interface, assuming secure coupling with the residual limb, while a distributed load of 100 N in the z-direction was

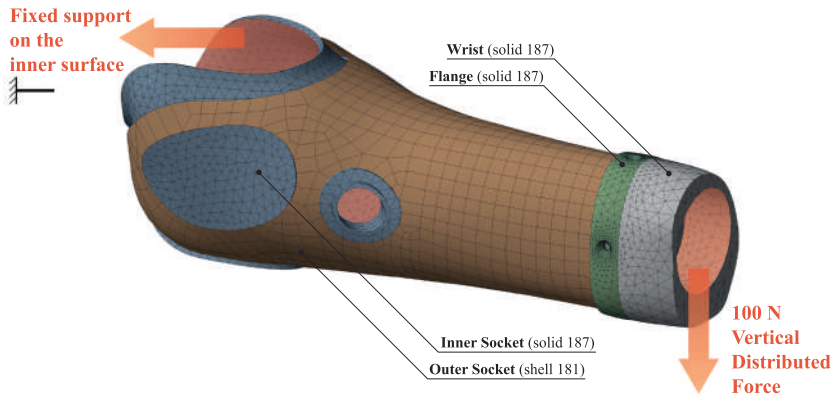

Fig. 5. Finite element model of the prosthetic socket, showing mesh discretization and boundary conditions. A fixed support was applied at the inner liner interface, and a 100 N distributed load was applied at the wrist housing to replicate a weightlifting scenario with a flexed elbow (90°).

applied at the wrist housing, mimicking the customer prescribed condition of weightlifting with a flexed elbow (90°). This value, conservative if compared to the actual maximum loads, was adopted as a reference. Alternative scenarios, similar to those studied by Mihcin et al. for the lower limb [60], such as dynamic loads on the upper limb during lifting, throwing, or rapid movements, accidental impacts, and daily activities like pushing, pulling, or carrying objects, could lead to different stress distributions and will be investigated in future studies.

The analysis was performed in ANSYS Mechanical APDL using a hybrid element approach: SOLID187 tetrahedral elements were used for the inner socket, flange, and wrist components, while SHELL181 elements modelled the lattice-based outer socket, which experiences primarily membrane actions. Mesh refinement was applied selectively, especially near bolt holes (element size = 1 mm), while a mesh dimension equal to the lattice cell dimension was set for the outer shell (element size = 7.8 mm) [61].

The FDD optimization followed the workflow shown in Fig. 6. First, a preliminary simulation was carried out, where uniform homogeneous material properties were imposed to shell elements representing the lattice structure. This initial simulation provided a preliminary stress map, which was subsequently imported in MATLAB. The stress value of each shell element was then used to assign a new homogenized material property associated with a thicker lattice structure. The association was performed thanks to a semi-proportional rule, where the stress distribution was divided into 16 intervals, as per Eq. (1).

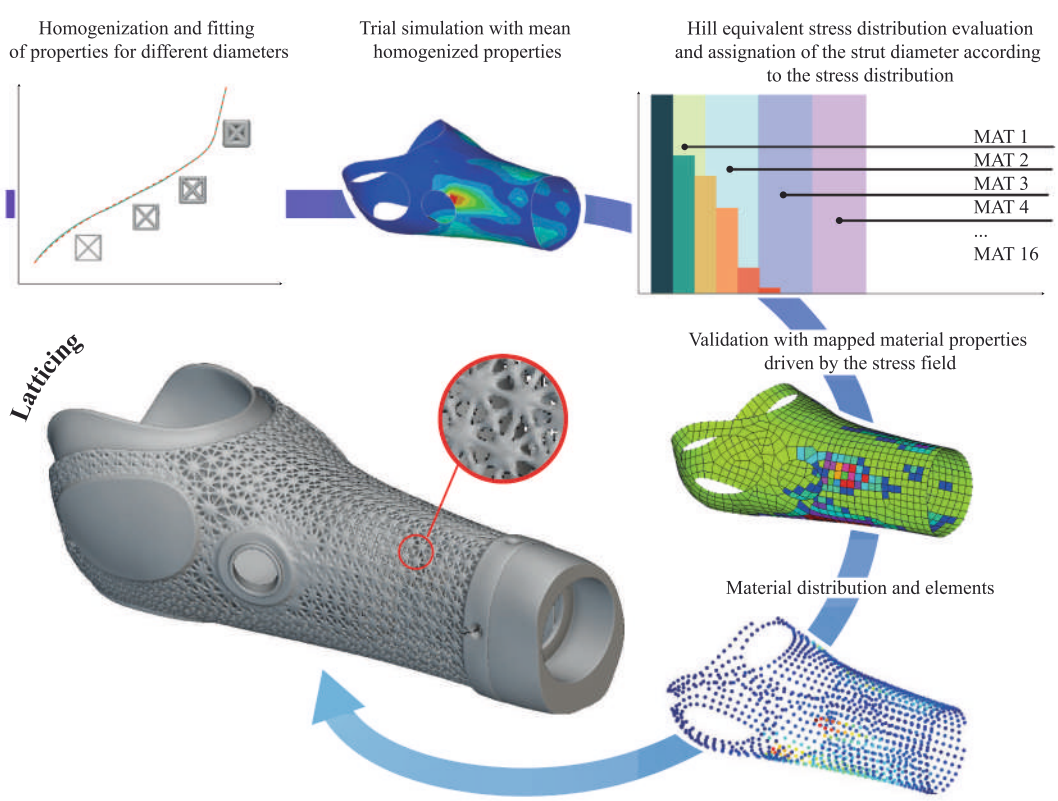

Fig. 6. Field-Driven Design workflow for the prosthetic socket. Finite element stress results were mapped to strut diameters through a MATLAB algorithm, generating a spatial diameter field. The graded lattice was then constructed in nTop and merged with the socket geometry, with fillets and blending applied at lattice-bulk interfaces to improve structural integrity.

$$\sigma_i = i\frac{\sigma_{MAX}}{16} \tag{1}$$

where $i = 1..16$, σ_i is the ith stress interval and σ_{MAX} is the maximum stress measure in the FE simulation. Each ith stress interval corresponds to one of the 16 material property sets obtained from the homogenization analysis of different strut diameters (d_i). The number of material-property intervals was limited by the effective manufacturing resolution of the MJF process, resulting in a 16-level discretization.

However, to ensure structural safety, printability, and robustness, a minimum strut diameter of 1.5 mm was imposed for elements experiencing stress levels below 25% of σ_{max}. This relation is formalized in Eq. (2):

$$d = \begin{cases} d_{min} if \sigma_i < 0.25\sigma_{max} \\ d_i if \sigma_i \geq 0.25\sigma_{max} \end{cases} \tag{2}$$

Low-stress regions (<25% of the maximum stress) were assigned a constant minimum strut diameter to reduce sensitivity to process-induced defects. The model, featuring the novel spatially varying homogenized material properties, was then solved to validate the performance of the graded lattice architecture. The final lattice structure was constructed in nTop (v2024, nTopology Inc., USA), following the stress-to-diameter field previously generated.

2.4. Lattice numerical models' validation

To validate numerically and experimentally the elastic–plastic homogenized material properties, two kinds of lattice specimens, i.e. the vertical specimen (V specimen) and the rotated specimen (R specimen), were designed as shown in Fig. 7. Both designs are representative of the lattice structure employed in the socket and the adopted RVEs are highlighted using dashed black lines. The RVE depicted in Fig. 7(a) was used to validate the uniaxial homogenized elastic–plastic mechanical properties along x and y directions, while the RVE rotated by 45° (Fig. 7 (b)) enabled the validation of homogenized elastic–plastic shear properties. This configuration enabled a complete analysis of the RVE orthotropic behaviour through simple tensile testing. In agreement with [58], lattice specimens were designed with three different zones: the central zone with constant strut diameter ($d = 1.4$ mm) and helix angle; the second zone, named as the transitional region, with variable strut diameter and helix angle, and the third zone as the bulk region where the clamping system was inserted during the tensile tests. The aim behind this type of design was to trigger the tensile failure in the central zone with constant strut diameter and helix angle similarly to failure of classical bulk specimens under tensile loadings. The tensile tests on the lattice specimens were performed at room temperature with an MTS servo hydraulic machine equipped with a load cell of 100 kN and an extensometer with an initial gauge length of $L_0 = 10mm$, mounted in the specimen midplane. The extensometer was clearly placed within the region with constant strut diameter.

Experimental data were compared with solid (i.e. with lattice cells) and homogenized FE elastic–plastic simulations of V and R specimens. To reduce the computational burden, FE simulations representing 1/20 of the V specimen and 1/14 of the R specimen were conducted, leveraging on geometrical symmetry as described in Fig. 7(c), for both homogenized and lattice geometries. Considering the roundness of the lattice specimens, as reported in Fig. 7, the homogenized models consisted of portions of cylinder that were constrained with symmetry

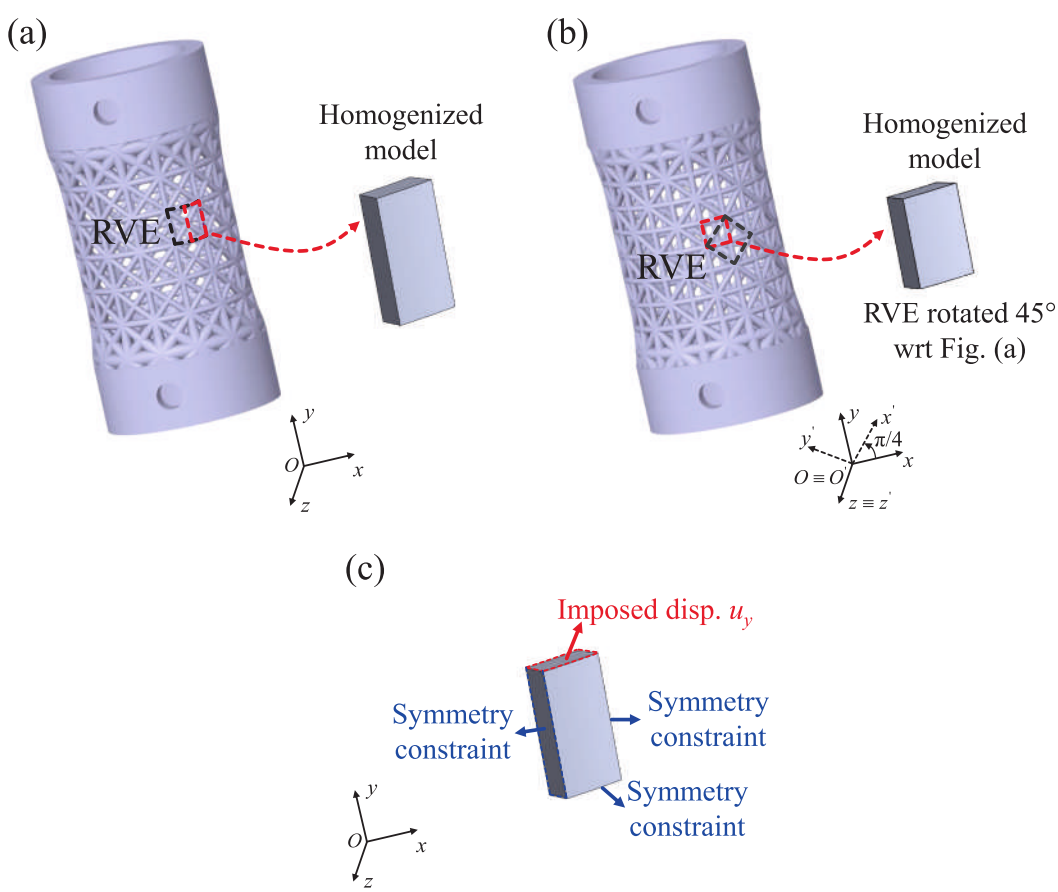

Fig. 7. Lattice specimen designs for experimental validation of the homogenization model: (a) vertical (V) specimen with struts aligned along the loading direction; (b) rotated (R) specimen with struts oriented at 45°. The central zones with constant strut diameter were used to trigger tensile failure under controlled conditions, while transitional and bulk regions enabled clamping during testing. (c) Constraints applied during FE simulations.

boundary conditions as shown in Fig. 7(c). Displacements were extracted at the strain gauge locations for solid and homogenized models to validate models' fitness. In particular, as concerns the FE simulation shown in Fig. 7(a), the orthotropic homogenized elastic–plastic mechanical properties obtained through the homogenization were defined as aligned with the reference system O presented in Fig. 7(a). On the contrary, given that the cell presented in Fig. 7(b) was rotated by 45° with respect to that of Fig. 7(a), the homogenized elastic–plastic properties were defined as aligned with the reference system O' in Fig. 7(b). This latter reference system was rotated by 45° with respect to z-axis of O.

2.5. Socket experimental validation

To validate the optimized socket, a single prototype was manufactured using the MJF technique, consistently with the procedure presented for tubular specimens in the previous section.

A complete three-dimensional computed tomography (CT) reconstruction was performed on the prototype to evaluate the manufacturing accuracy. This technique enabled a non-destructive metrological inspection of the socket in the as-built condition. CT scans were acquired with a Zeiss Metrotom system (parameters reported in Table 1), and the three-dimensional reconstruction of the socket geometry was analysed using ORS-*Dragon*fly software (Comet Technologies Canada Inc., Canada).

The socket was then tested under bending, in a set-up able to replicate the conditions of the use case identified in the FE analysis presented in Fig. 5. To obtain this nonstandard setup, a custom suspension system was designed, composed of a "L" shaped support, in aluminium alloy, and an AM PA12 flanged hollow cylinder able to host the specimen. The socket was kept in place thanks to three bolted connections, as shown in Fig. 8, between the PA12 flanged hollow cylinder and the bulk patches (non-lattice regions) on the outer part of the socket. Three pairs of supporting parts were additionally manufactured, still in PA12, to accommodate two bolts for each gripping non-lattice region. These parts were obtained by replicating the shape of the socket surfaces and the inner cylinder surface, Fig. 8(c). The bulk patches of the specimen were drilled during assembly, while the supporting parts served as positioning fixtures for the drilling operation. The set-up did not replicate the exact configuration of a socket under normal operating conditions, as a direct and robust connection between the testing machine and the internal socket proved too challenging to achieve. However, this solution reproduced the loading conditions acting on the lattice structure during use. It therefore represents a trade-off, enabling accurate loading of the most critical components – namely the lattice structure – while ensuring a stiff connection, a reliable and reproducible testing configuration. Vertical load was applied on a custom wrist with a servo-hydraulic Walter Bai Type LFV testing machine, equipped with a 25kN load cell. Testing speed was set equal to 0.6 mm/min, and to have the orientation of the load upward, the socket was oriented upside down with respect to its natural orientation in use.

3. Results and discussion

3.1. Results of elastic–plastic homogenization

To characterize the mechanical behaviour of lattice structure with different relative density, several elastic–plastic FE homogenization simulations were performed. Results are presented in Fig. 9 where the uniaxial response along x direction and the shear response in xy plane are reported vs the strut diameter variation. Results of the homogenized elastic–plastic quantities are reported in Table 2.

Appendix B in the supplementary material section shows that the unit cell behaves as an in-plane square orthotropic material, requiring E, ν, and g to describe the elastic homogenized response. For the plastic response, the Hill yielding rule for in-plane square orthotropy is given by Eq. (3), with the constants to be identified being H, N, and the initial yield σ_0. As shown in Table 2, as the strut diameter increases, the homogenized Young's modulus tends to the bulk value of 1120 MPa, reflecting a transition toward a continuum-like RVE. The Poisson ratio ν initially decreases and then increases for diameters >2.5 mm, approaching 0.40 at large diameters; this trend is explained by the reduced influence of the X-shaped interior's bending stiffness at small diameters and its increasing stiffness at larger diameters. Beyond 2.5 mm, the unit cell resembles a continuum, diminishing the relevance of the X-bending stiffness in determining ν, which converges to the continuum value. The same rationale applies to G, which tends toward $g \approx E/[2(1+\nu)]$ at large diameters, indicating convergence to isotropic continuum behaviour. Similar considerations hold for the homogenized plastic properties. The homogenized σ_0 tends toward the bulk value reported in prior work [49], while H and N converge to 0.5 and 1.5, respectively; in fact, by increasing diameter, Hill yielding criterion converges to Von Mises yielding rule, i.e., $H = 0.5$ and $N = 1.5$

$$\sigma_{eq} = \sqrt{\sigma_{xx}^2 + \sigma_{yy}^2 - 2H\sigma_{xx}\sigma_{yy} + 2N\tau_{xy}^2} \tag{3}$$

To ensure uniform distribution of mechanical properties, a fifth-degree polynomial regression was applied to fit the elastic, shear, and Poisson's ratio data as functions of diameter. Due to the non-linear relationship between diameter and mechanical performance, the regression function was inverted to assign diameters based on equidistant mechanical property intervals rather than diameter intervals. This inversion allowed the derivation of 16 evenly spaced material property sets, ensuring better alignment with the stress spectrum extracted from FEA, as shown in Fig. 10.

3.2. Socket simulation results and Field-Driven design model (FDDM)

Building on the elastic–plastic homogenized properties and on the FDD procedure, the socket underwent a stress-driven design process. The initial uniform simulation was performed with homogenized average lattice properties, and the stress evaluation was based on the Hill yielding criterion, as per Eq. (3). The resulting stress field (Fig. 11(a)) guided the Field-Driven workflow, which assigned locally varying material properties to shell elements.

Due to APDL limitations in handling Hill stresses with element-dependent parameters (N and σ_0), the stress analysis of the FDDM was carried out in MATLAB. The mapped material distribution (Fig. 11(b)) produced the Hill stress and safety factor fields shown in Fig. 11(c and d). The maximum homogenized stress reached 2.1 MPa, while the safety factor ranged from 4.2 to more than 10. As shown in Fig. 11(d), the minimum safety factors were located at the interface between the lattice shell and the bulk regions, where the transition from porous metamaterial to solid geometry introduces an intrinsic geometric discontinuity. Despite this geometrical feature, the gradual transition between a bulk to a porous geometry provided by the stress-driven design allowed safety factors with a large margin, providing strong reassurance of its mechanical reliability under prescribed loading conditions.

Table 3 summarizes the optimization results by comparing the structural performance of the bulk socket, the lattice prosthetic with uniform properties, and the FDDM-based design. The mean properties model employed uniform struts of approximately 2.5 mm in diameter, whereas the FDDM primarily featured thinner struts (~1.4 mm) with localized enlargements in high-stress regions. The smaller strut diameters in the FDDM design resulted in reduced stiffness and increased

Table 1
CT scanning parameters adapted for the socket geometrical reconstruction.

Voltage – kV	Current – μA	Voxel size – μm	Cu physical filter – mm	Nr. projections
200	1000	127	0.25	2050

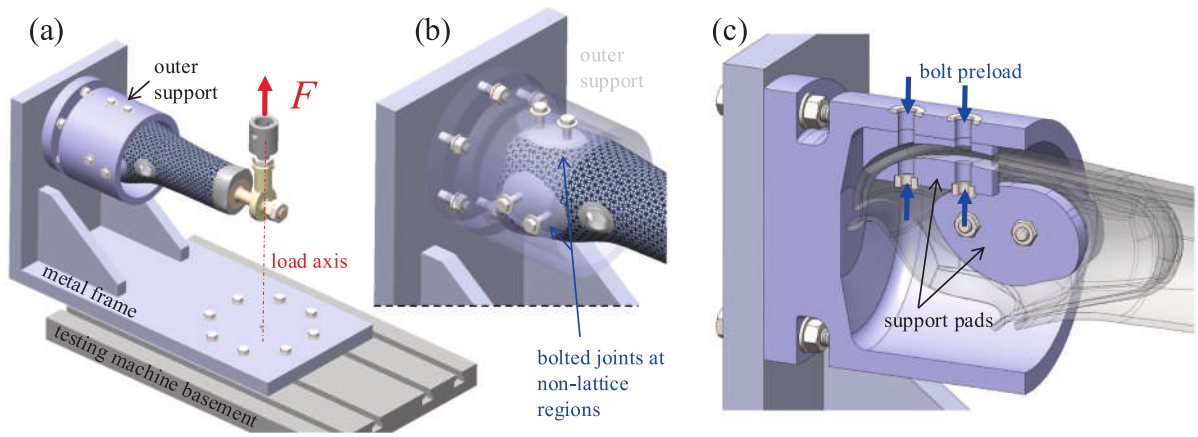

Fig. 8. (a) Overall view of the frame and the socket, for the bending test, with the load axis aligned to the testing machine actuator. (b) Bolted regions to connect the socket with the flanged outer support. (c) Bolt preload applied to the gripping non-lattice regions, acting by means of support pads designed with specific shapes.

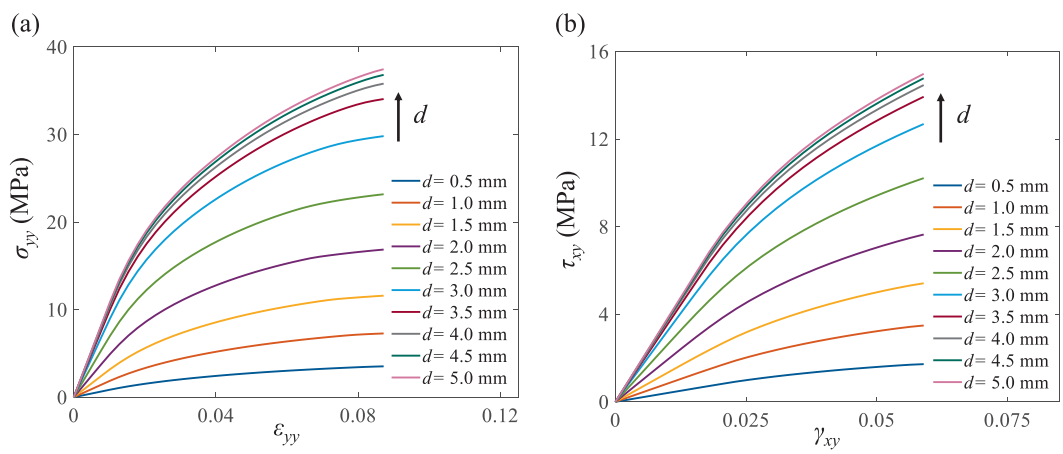

Fig. 9. Results of elastic–plastic finite element simulations of the representative volume element (RVE): (a) uniaxial loading along the y-direction; (b) shear loading in the xy-plane. These simulations were performed across different strut diameters and used to derive the homogenized elastic–plastic properties of the lattice structures.

Table 2
Homogenized elastic–plastic properties of the RVE by varying strut diameter.

Diameter d (mm)	E (MPa)	N	G (MPa)	H	N	σ_0 (MPa)
0.5	84.0	0.430	40.4	0.821	0.883	1.11
1.0	184	0.426	83.5	0.809	1.04	2.38
1.5	314	0.404	133	0.746	1.22	3.93
2.0	488	0.374	193	0.704	1.31	5.90
2.5	694	0.362	262	0.632	1.36	7.53
3.0	885	0.376	324	0.598	1.41	10.1
3.5	982	0.388	355	0.571	1.42	11.5
4.0	1030	0.392	368	0.554	1.45	12.2
4.5	1050	0.395	376	0.537	1.46	12.6
5.0	1070	0.397	382	0.525	1.48	12.8

localized stresses, particularly in critical regions such as the access hole for removal of the wearing scabbard. Nevertheless, the FDDM achieved a 25.4% weight reduction compared to the bulk design and a 13.2% reduction relative to the mean-properties model. Both the mean-properties and FDDM sockets exhibited sufficient mechanical strength under the prescribed loading conditions, representative of critical daily use scenarios. Although slightly higher deformations were observed – still within acceptable limits for prosthetic applications – the FDDM maintained a satisfactory safety factor while significantly reducing weight, supporting its potential for clinical implementation.

The present study considered also user-centred aspects such as comfort, breathability, weight distribution, and integration of electronics. However, the ergonomic observation, conducted on a single user, remains preliminary and qualitative, while clinical validation has yet to be performed.

3.3. Socket metrological analysis

The FDDM socket was manufactured as shown in Fig. 12(a). The three-dimensional CT-based geometrical reconstruction was focused on the distal area of the socket (Fig. 12(b)), which is mainly characterized by struts with the minimum as-designed cross-section. The colormap shows the strut dimensions obtained from CT reconstruction. An equivalent analysis was performed on the as-designed CAD geometry, with the results reported in Fig. 12(c) and (d). The frequency of struts with diameters below 1.3 mm was minimal in the CT-reconstructed geometry, and nearly zero below 1.4 mm in the CAD model. Instances of elements measured below the nominal minimum diameter in the CAD histogram were attributed to mesh-edge imperfections during the region-of-interest selection. The modal diameters were approximately 1.4 mm for the CT-reconstructed geometry and 1.5 mm for the CAD model. Overall, the CT results showed good agreement with the as-designed geometry, with only a slight shift toward smaller diameters; however, both distributions fell within the uncertainty range imposed by the CT voxel size. This confirms the manufacturability of the proposed design using an industrially relevant process, supporting its

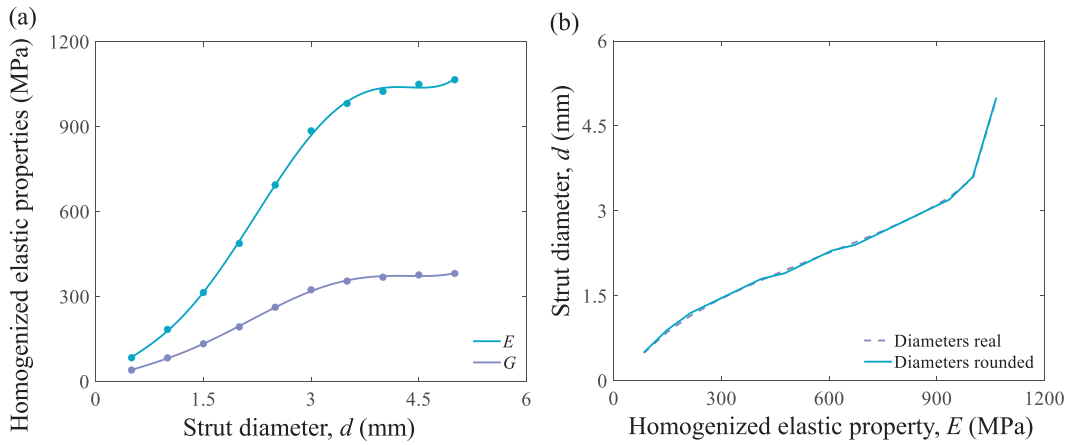

Fig. 10. Inversion of the fitting function relating strut diameter to mechanical properties. The regression was reformulated to generate evenly spaced elastic property intervals, enabling consistent assignment of strut diameters across the stress spectrum.

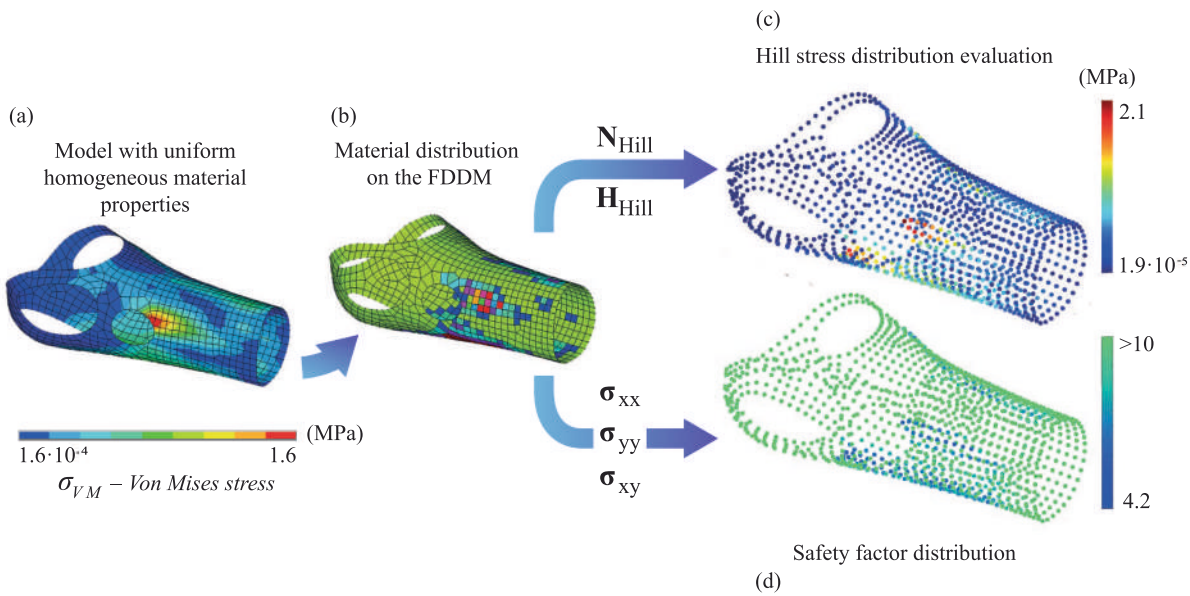

Fig. 11. Stress field obtained from the simulation using the mean-property model (a). Mapped material distribution generated by the FDD workflow (b). FDDM solution showing the assignment of the Hill coefficients, together with the resulting stress and safety factor distributions (c–d).

Table 3
Comparison among the bulk model, mean properties model, and Field-Driven Design Model (FDDM) in terms of weight, vertical deflection (stiffness), and equivalent Hill stress with associated safety factors. The FDDM achieved a 25.4% weight reduction compared to the bulk design and a 13.2% reduction compared to the mean properties model, while maintaining adequate stiffness and safety margins.

	Bulk model	Mean property model	FDD model
Weight (g)	500	434	373
Weight reduction (%)	0	13.2	25.4
Max anterior deflection (mm)	0.7	1.1	1.6
Max Hill stress (MPa)	1.64	1.67	2.1
Min safety factor	6.7	4.5	4.2

transfer toward practical industrial applications.

3.4. Elastic–plastic homogenization validation

Elastic-plastic homogenization was validated both numerically and experimentally. The experimental results of the tensile tests on V and R specimens are presented in Fig. 13(a) and (b). The ending points of the average experimental curves were defined by considering the minimum value of the maximum strain at failure of the tested specimens. Two pictures of the clamping system used during tensile tests are also reported in Fig. 13, and as designed in [58] to guarantee a secure hold and prevent slippage during all stages of tensile testing. The results of the tests in terms of ultimate strength and strain at fracture of the average experimental curves were very similar. The dispersion of the results of the test was low and slightly higher in the R specimens than V specimens.

The comparison between the experimental data and the FE simulations of the lattice specimens and of the homogenized models are reported in Fig. 13(c) and (d) for the two specimens. The results highlight the strong correlation between FE results of the homogenized and lattice models and the average experimental curves. As V specimens are concerned, both homogenized and lattice FE results were slightly lower than the corresponding average experimental curve, while the FE results of homogenized and lattice models of R specimens were almost perfectly superimposed on the experimental data. The results of V and R specimens provided a complete validation of the obtained elastic–plastic

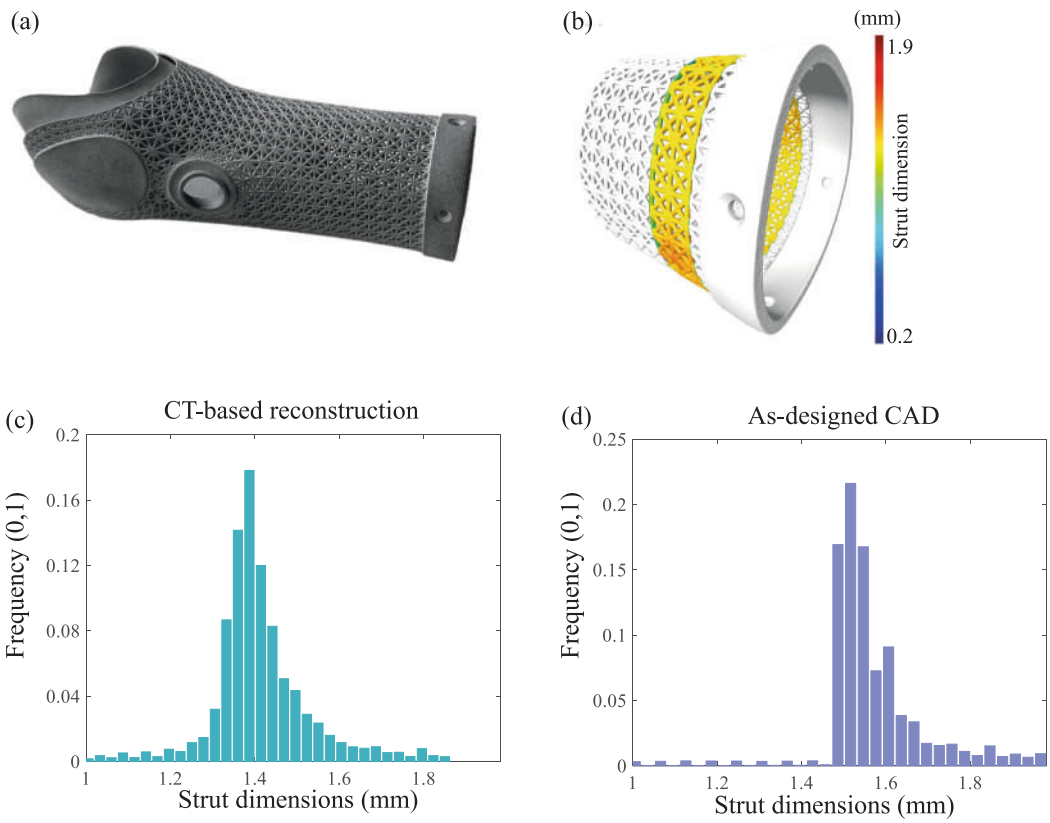

Fig. 12. Additively manufactured prosthetic socket and dimensional validation: (a) socket fabricated by Multi Jet Fusion (MJF); (b) CT-based geometrical reconstruction of the distal region, showing the strut dimensions; (c) statistical distribution of strut diameters obtained from the CT reconstruction; and (d) corresponding distribution from the as-designed CAD model. The results confirm good agreement between the designed and manufactured geometries, with only a slight shift towards smaller diameters in the printed structure.

homogenized uniaxial properties along y and *x* axes and of shear properties, respectively. Overall, the low dispersion of the experimental data and the overlap between FE results, by using as-design geometries, and experimental data emphasize the high repeatability and manufacturing accuracy provided by MJF 3D printing technique and the suitability of PA12 for this latter manufacturing process.

3.5. Socket experimental validation

Fig. 14 depicts the force–displacement response of the socket prototype subjected to quasi-static loading. The relation was characterized by an initial linear trend followed by a limited plateau before the final failure. The component did not present a large plastic plateau – a characteristic shared also by tubular lattice specimens – and the associated load was equivalent to the one measured at the force at failure. The value of the force measured in this condition was 440 N, largely above the 100 N identified as critical in the FE model. Interestingly, a close agreement was observed in the safety factors measured during the FE simulation and this experimental validation: the minimum predicted safety factor in the model was 4.2 while the experimental one was 4.4. This agreement strongly supports the FE homogenized model proposed, and paves the way for a more complex, and industrially relevant application of lattice structures in the design of prosthetic devices. The readers should interpret the presented data not as a complete validation of the prosthetic design, which would require correlation with patient-reported outcomes as well as durability and fatigue assessments, but rather as a consistent validation of the finite element tool developed in this work.

4. Conclusions and future perspectives

This work presented a novel methodology for design, fabrication and testing of prosthetic sockets based on Field-Driven lattice architecture. In this paper, we focused on establishing the overall methodology, verifying mechanical strength, and manufacturability as a prerequisite for future clinical investigation, that are beyond the scope of this work. The proposed approach integrated finite element stress mapping, homogenization-based property assignment, advanced additive manufacturing, and experimental validation to enable the generation of lightweight, anatomically compatible, and mechanically reliable socket structures.

Metrological validation using computed tomography confirmed the manufacturability of the graded lattice design with industrially relevant processes, showing good agreement between the as-designed and as-built geometries. Numerical analyses demonstrated that the Field-Driven Design Model (FDDM) achieved significant weight reduction (up to 25.4% compared to the bulk design) while maintaining sufficient stiffness and a reassuringly high safety factor under representative loading scenarios. Experimental testing on a full-scale prototype of the socket showed satisfactory [62] agreement between the FE predictions, proving the validity of the proposed homogenized modelling strategy and the structural soundness of the design under a simplified scenario of everyday-life loading conditions.

A single-subject case study was adopted to demonstrate the feasibility of the personalized digital workflow, although human-in-the-loop refinements were still required to achieve a satisfactory fit. All together, these results provided a proof of concept for the proposed approach and support the use of Field-Driven lattice Design for lightweight prosthetic socket development.

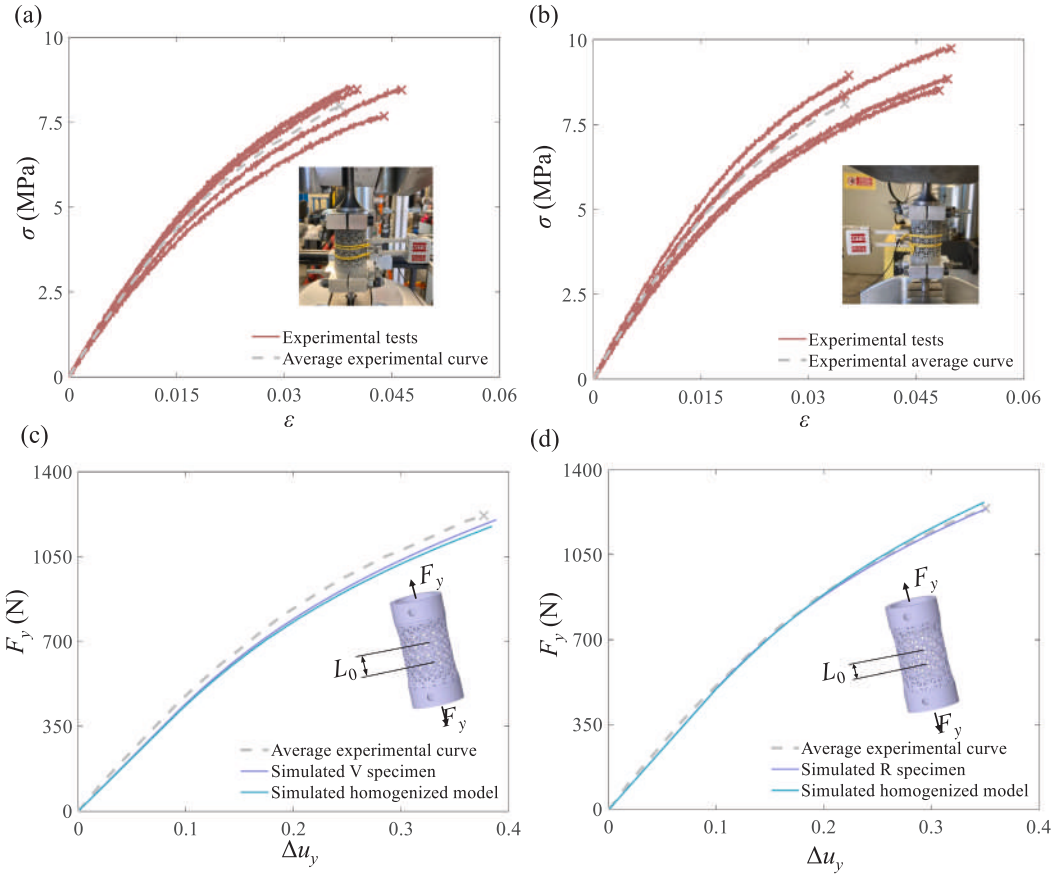

Fig. 13. Results of tensile tests on lattice specimens: (a) V specimen and (b) R specimen. The experimental data are plotted in solid red line, while the average is represented in light grey dashed line. Comparison between experimental data (dashed light grey line) and FE results of simulations of entire lattice specimens (solid violet line) and homogenized model (solid aquamarine line) for the V specimen (c) and R specimen (d). (For interpretation of the references to colour in this figure legend, the reader is referred to the web version of this article.)

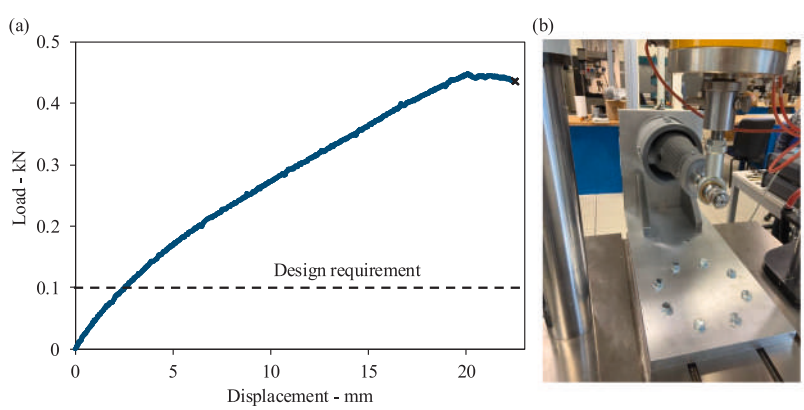

Fig. 14. (a) Quasi static force–displacement relation for AM lattice based optimized socket and (b) picture of the experimental set-up.

Future work will extend the proposed methodology to account for manufacturing imperfections and fatigue behaviour, by investigating the combined effects of process-induced defects, geometrical deviations, and cyclic loading on the long-term mechanical performance of the socket. When complex components are subjected to cyclic loading scenario, such as in this case, a specific study on fatigue failure is mandatory. For this reason, a complete fatigue verification on prototypes needs to be performed as future development. Specifically, thanks to the experimental set-up developed in this work, the future steps will be devoted to applying the Average Strain Energy Density framework developed in [63] to predict the fatigue resistance of lattice-based components. In addition, patient-specific optimization will be pursued through the integration of anatomical data and user-specific functional requirements into the automated design pipeline, enabling the development of fully personalized sockets. Clinical validation will be then carried out through long-term experimental trials with users, aimed at assessing comfort, usability, and durability under daily use. Finally, the proposed Field-Driven lattice framework will be explored for broader applications, including its transfer to other biomedical devices and lightweight engineering components. Overall, this study lays the

groundwork for a new generation of prosthetic sockets that combine advanced structural design with industrially viable additive manufacturing, bridging the gap between engineering innovation and patient-centred healthcare, while providing a foundation for future regulatory-compliant implementation in clinical and practical applications (e.g., ISO 13485/MDR) [64].

CRediT authorship contribution statement

P. Borracci: Writing – original draft, Visualization, Validation, Software, Methodology, Investigation, Formal analysis, Data curation. **D. Menel:** Writing – original draft, Visualization, Validation, Software, Methodology, Investigation, Formal analysis, Data curation. **L. Romanelli:** Data curation, Formal analysis, Investigation, Methodology, Software, Validation, Writing – original draft, Visualization. **R. De Biasi:** Writing – review & editing, Visualization, Validation, Software, Methodology, Investigation, Formal analysis, Data curation. **F. Napoleoni:** Writing – review & editing, Validation, Methodology, Investigation, Formal analysis. **I. Senegaglia:** Writing – review & editing, Validation, Methodology, Investigation, Formal analysis. **P. Neri:** Writing – review & editing, Methodology, Investigation, Formal analysis. **C. Santus:** Writing – review & editing, Visualization, Supervision, Resources, Methodology, Investigation, Funding acquisition, Formal analysis, Conceptualization. **M. Controzzi:** Writing – review & editing, Visualization, Supervision, Resources, Project administration, Methodology, Investigation, Funding acquisition, Formal analysis, Conceptualization. **M. Benedetti:** Writing – review & editing, Visualization, Supervision, Resources, Project administration, Methodology, Investigation, Funding acquisition, Formal analysis, Conceptualization.

Declaration of Generative AI and AI-assisted technologies in the writing process

During the preparation of this work the author(s) used Grammarly, Chat-GPT, Gemini, in order to proofread the manuscript and improve the readability. After using this tool/service, the author(s) reviewed and edited the content as needed and take(s) full responsibility for the content of the published article.

Declaration of competing interest

The authors declare that they have no known competing financial interests or personal relationships that could have appeared to influence the work reported in this paper.

Acknowledgments

This work was Funded by the European Union - Next Generation EU and supported by the Italian Ministry of University and Research (MUR) in the frame of the programme PRIN 2022 (Avviso DD 104 del 02/02/22) Piano Nazionale di Ripresa e Resilienza (PNRR) – Missione 4 Componente 2, ‘‘Dalla ricerca all’impresa’’ Investimento 1.1, ‘‘Fondo per il Programma Nazionale di Ricerca e Progetti di Rilevante Interesse Nazionale (PRIN), project title ‘‘Calliope: lattiCe bAsed uLtra Light SensOrized upper limb ProsthEsis’’, grant number 2022PRHZM3 - CUP J53D23002380001 (CUP University of Pisa unit I53D23001840006).

Link to the website of the project: https://www.calliope-hand.it/.

Appendix A. Supplementary data

Supplementary data to this article can be found online at https://doi.org/10.1016/j.matdes.2026.116509.

Data availability

Data are available from the corresponding authors and made available upon reasonable request.

References

[1] J. Olsen, S. Day, S. Dupan, K. Nazarpour, M. Dyson, 3D-printing and upper-limb prosthetic sockets; promises and pitfalls, IEEE Trans. Neural Syst. Rehabil. Eng. 29 (2021) 527–535, https://doi.org/10.1109/TNSRE.2021.3057984.

[2] The Leeds Teaching Hospitals NHS. The prosthetic limb service, 2012. https://www.leedsth.nhs.uk/assets/Uploads/fc3D0ec95f/Out-patient-Leaflet-1.pdf.

[3] N. Herbert, D. Simpson, W. Spence, W. Ion, A preliminary investigation into the development of 3-D printing of prosthetic sockets, J. Rehabil. Res. Dev. 42 (2005) 141–146, https://doi.org/10.1682/JRRD.2004.08.0134.

[4] M.J. Quigley, The role of test socket procedures in today’s prosthetic practice, J. Prosthet. Orthot. 9 (3) (1985) 11–12. http://www.oandplibrary.org/cpo/pdf/1985_03_011.pdf.

[5] A. Mehboob, I. Barsoum, R.K. Abu Al-Rub, Review on lower limb bone fracture fixation: biomechanics, design, and advancements in additive manufacturing for implants, Mater. Des. 260 (2025) 115001, https://doi.org/10.1016/j.matdes.2025.115001.

[6] A.M. Gómez-Amador, C. Pérez-Carrera, L. Prieto-Fernández, H. Rubio-Alonso, 3D-printed prosthetic foot design: Mechanical similarity and testing, Mater. Des. 253 (2025) 113918, https://doi.org/10.1016/j.matdes.2025.113918.

[7] F. Liu, Y. Shao, M. Chen, Generative design strategies for additive manufacturing of lattice structures: a review, Mater. Des. 262 (2026) 115431, https://doi.org/10.1016/j.matdes.2026.115431.

[8] Unlimited Tomorrow. *TrueLimb* [Internet]. [cited 2025 Jul 29]. Available from: https://www.unlimitedtomorrow.com/truelimb/.

[9] Open Bionics. Hero Arm [Internet]. [cited 2025 Jul 29]. Available from: https://openbionics.com/hero-arm/.

[10] M.M. Rodgers, G. Alon, V.M. Pai, R.S. Conroy, Wearable technologies for active living and rehabilitation: current research challenges and future opportunities, J. Rehabil. Assist. Technol. Eng. 6 (2019) 1–9, https://doi.org/10.1177/2055668319839607.

[11] A. G. Cutti, E. Casamenti, A. Cappello, A. Davalli, A simplified cad model of trans-radial sockets suitable for subject energy expenditure assessment, in: Proceedings of the MEC’05 Conference, 2005, UNB, https://hdl.handle.net/10161/2703.

[12] M. Benedetti, A. Du Plessis, R.O. Ritchie, M. Dallago, N. Razavi, F. Berto, Architected cellular materials: a review on their mechanical properties towards fatigue-tolerant design and fabrication, Mater. Sci. Eng. R. Rep. 144 (2021) 100606, https://doi.org/10.1016/j.mser.2021.100606.

[13] S. Arabnejad, B. Johnston, M. Tanzer, D. Pasini, Fully porous 3D printed titanium femoral stem to reduce stress-shielding following total hip arthroplasty, J. Orthop. Res. Soc. 35 (8) (2017) 1774–1783, https://doi.org/10.1002/jor.23445.

[14] M.F. Ashby, The properties of foams and lattices, Philos. Trans. A Math. Phys. Eng. Sci. 364 (1838) (2006) 15–30, https://doi.org/10.1098/rsta.2005.1678. PMID: 18272451.

[15] Y. Liang, W. Zhou, Y. Liu, Z. Li, Y. Yang, H. Xi, Z. Wu, Energy absorption and deformation behavior of 3D printed triply periodic minimal surface stainless steel cellular structures under compression, Steel Res. Int. 92 (2021) 2000411, https://doi.org/10.1002/srin.202000411.

[16] O. Al-Ketan, D.W. Lee, R. Rowshan, R.K. Abu Al-Rub, Functionally graded and multi-morphology sheet TPMS lattices: design, manufacturing, and mechanical properties, J. Mech. Behav. Biomed. Mater. 102 (2020 Feb) 103520, https://doi.org/10.1016/j.jmbbm.2019.103520. Epub 2019 Nov 5 PMID: 31877523.

[17] Y. Liu, Mechanical properties of a new type of plate–lattice structures, Int. J. Mech. Sci. 192 (2021) 106141, https://doi.org/10.1016/j.ijmecsci.2020.106141.

[18] T. Tancogne-Dejean, M. Diamantopoulou, M.B. Gorji, C. Bonatti, D. Mohr, Adv. Mater. 30 (2018) 1803334, https://doi.org/10.1002/adma.201803334.

[19] C. Bhat, M.J. Prajapati, A. Kumar, J.-Y. Jeng, Additive manufacturing-enabled advanced design and process strategies for multi-functional lattice structures, Materials 17 (14) (2024) 3398, https://doi.org/10.3390/ma17143398.

[20] A. Kumar, L. Collini, C. Ursini, J.-Y. Jeng, Energy absorption and stiffness of thin and thick-walled closed-cell 3D-printed structures fabricated from a hyperelastic soft polymer, Materials 15 (7) (2022) 2441, https://doi.org/10.3390/ma15072441.

[21] C. Bhat, A. Kumar, S. Lin, J. Jeng, A novel bioinspired architectured materials with interlocking designs based on tessellation, Addit. Manuf. 58 (2022) 103052, https://doi.org/10.1016/j.addma.2022.103052.

[22] R. Hill, Elastic properties of reinforced solids: some theoretical principles, J. Mech. Phys. Solids 11 (5) (1963) 357–372, https://doi.org/10.1016/0022-5096(63)90036-X.

[23] P. Suquet, Elements of homogenization for inelastic solid mechanics, in: E. Sanchez-Palencia, A. Zaoui (Eds.), Homogenization Techniques for Composite Media (lecture Notes in Physics, vol. 272, Springer-Verlag, 1987, pp. 193–278.

[24] B.B. Babamiri, H. Askari, K. Hazeli, Deformation mechanisms and post-yielding behavior of additively manufactured lattice structures, Mater. Des. 188 (2020) 108443, https://doi.org/10.1016/j.matdes.2019.108443.

[25] V.S. Deshpande, N.A. Fleck, Isotropic constitutive models for metallic foams, J. Mech. Phys. Solids 48 (6-7) (2000) 1253–1283, https://doi.org/10.1016/s0022-5096(99)00082-4.

[26] K. Ushijima, W.J. Cantwell, D.H. Chen, Prediction of the mechanical properties of micro-lattice structures subjected to multi-axial loading, Int. J. Mech. Sci. 68 (2013) 47–55, https://doi.org/10.1016/j.ijmecsci.2012.12.017.

[27] T. Tancogne-Dejean, D. Mohr, Elastically-isotropic truss lattice materials of reduced plastic anisotropy, Int. J. Solids Struct. 138 (2018) 24–39, https://doi.org/10.1016/j.ijsolstr.2017.12.025.
[28] M. Mahbod, M. Asgari, Elastic and plastic characterization of a newly developed additively manufactured functionally graded porous lattice structure: analytical and numerical models, Int. J. Mech. Sci. 155 (2019) 248–266, https://doi.org/10.1016/j.ijmecsci.2019.02.041.
[29] M. Eynbeygui, J. Arghavani, A.H. Akbarzadeh, R. Naghdabadi, Anisotropic elastic-plastic behavior of architected pyramidal lattice materials, Acta Mater. 183 (2020) 118–136, https://doi.org/10.1016/j.actamat.2019.10.038.
[30] O. Weeger, I. Valizadeh, Y. Mistry, D. Bhate, Inelastic finite deformation beam modeling, simulation, and validation of additively manufactured lattice structures, Addit. Manuf. Lett. 4 (2023) 100111, https://doi.org/10.1016/j.addlet.2022.100111.
[31] J. Schneider, S. Kumar, Comparative performance evaluation of microarchitected lattices processed via SLS, MJ, and DLP 3D printing methods: experimental investigation and modelling, J. Mater. Res. Technol. 26 (2023) 7182–7198, https://doi.org/10.1016/j.jmrt.2023.09.061.
[32] K. Somlo, S.S. Chauhan, C.F. Niordson, K. Poulios, Uniaxial tensile behaviour of additively manufactured elastically isotropic truss lattices made of 316L, Int. J. Solids Struct. 246–247 (2022) 111599, https://doi.org/10.1016/j.ijsolstr.2022.111599.
[33] Y. Wang, S. Li, Y. Yub, Y. Xin, X. Zhang, Q. Zhang, S. Wang, Lattice structure design optimization coupling anisotropy and constraints of additive manufacturing, Mater. Des. 196 (2020) 109089, https://doi.org/10.1016/j.matdes.2020.109089.
[34] M. Yao, P. Wang, S. Wang, M. Zhu, M. Tang, Multi-objective field-based collaborative design of multi-layer IWP lattice enhancement mechanisms and mechanical properties, Mater. Des. 263 (2026) 115588, https://doi.org/10.1016/j.matdes.2026.115588.
[35] G. Allen, Field-Driven Design Whitepaper, nTop Learning Center. [Online]. Available at: https://www.ntop.com/resources/guides/download-whitepaper-field-driven-design/.
[36] M.P. Bendsoe, O. Sigmund, Topology Optimization: Theory, Methods, and Applications, Springer Science & Business Media, 2013.
[37] J. Gu, S. Naqvi, L. Naqvi, C. Chao, Y. Jiao, M.A. Yang, Z. Nasir, L. Tian, D. Shen, H. L. Wang, Stress-driven design method for porous maxillofacial prosthesis based on triply periodic minimal surface, Compos. Struct. 355 (2025) 118863, https://doi.org/10.1016/j.compstruct.2025.118863.
[38] M. Fraldi, L. Esposito, G. Perrella, A. Cutolo, S.C. Cowin, Topological optimization in hip prosthesis design, Biomech. Model. Mechanobiol. 9 (4) (2010) 389–402, https://doi.org/10.1007/s10237-009-0183-0.
[39] O. Ozmen, H.K. Surmen, Design of 3D printed below-knee prosthetic - a finite element and topology optimization study, Stroj. Vestn. J. Mech. Eng. 70 (11-12) (2024) 517–530, https://doi.org/10.5545/sv-jme.2024.1034.
[40] M. Amirpour, E. Feng, A. Entezari, A hybrid CFD–machine learning framework for efficient permeability prediction in 3D-printed bone scaffold design, Mater. Today Commun. 52 (2026), https://doi.org/10.1016/j.mtcomm.2026.114992.
[41] L. Paternò, M. Ibrahimi, E. Gruppioni, A. Menciassi, L. Ricotti, Sockets for limb prostheses: a review of existing technologies and open challenges, I.E.E.E. Trans. Biomed. Eng. 65 (9) (2018) 1996–2010, https://doi.org/10.1109/TBME.2017.2775100.
[42] C. Lake, The evolution of upper limb prosthetic socket design, JPO J. Prosthet. Orthot. 20 (2008) 85–92, https://doi.org/10.1097/JPO.0b013e31817d2f08.
[43] D. Sengeh, M.S. Moinina, H. Herr, A variable-impedance prosthetic socket for a transtibial amputee designed from magnetic resonance imaging data, JPO J. Prosthet. Orthot. 25 (3) (2013) 129–137, https://doi.org/10.1097/JPO.0b013e31829be19c.
[44] K. Moerman, D. Sengeh, H. Herr, Automated and data-driven computational design of patient-specific biomechanical interfaces (2016). https://doi.org/10.31224/osf.io/g8h9n.
[45] G. Facoetti, S. Gabbiadini, G. Colombo, C. Rizzi, Knowledge-based system for guided modeling of sockets for lower limb prostheses, CAD Appl. 7 (2010) 723–737, https://doi.org/10.3722/cadaps.2010.723-737.
[46] N.C. Paxton, R.C. Nightingale, M.A. Woodruff, Capturing patient anatomy for designing and manufacturing personalized prostheses, Curr. Opin. Biotechnol. 73 (2022) 282–289, https://doi.org/10.1016/j.copbio.2021.09.004.
[47] Borthakur, Partha, The role and future directions of 3D printing in custom prosthetic design 10 (2025). https://doi.org/10.3390/engproc2024081010.
[48] D.G. Smith, E.M. Burgess, The use of CAD/CAM technology in prosthetics and orthotics—current clinical models and a view to the future, J. Rehabil. Res. Dev. 38 (2001) 327–334.
[49] F. Górski, R. Wichniarek, W. Kuczko, M. Żukowska, Study on properties of automatically designed 3D-printed customized prosthetic sockets, Mater 14 (18) (2021) 5240, https://doi.org/10.3390/ma14185240.
[50] Y. Wang, Q. Tan, F. Pu, D. Boone, M. Zhang, A review of the application of additive manufacturing in prosthetic and orthotic clinics from a biomechanical perspective, Engineering 6 (2020) 1258–1266, https://doi.org/10.1016/j.eng.2020.07.019.
[51] X. Yang, R. Zhao, D. Solav, X. Yang, D.R.C. Lee, B. Sparrman, Y. Fan, H. Herr, Material, design, and fabrication of custom prosthetic liners for lower-extremity amputees: a review, Med. Novel Technol. Dev. 17 (2023) 100197, https://doi.org/10.1016/j.medntd.2022.100197.
[52] F. Górski, R. Wichniarek, W. Kuczko, M. Żukowska, E. Suszek, Rapid manufacturing of individualized prosthetic sockets, Adv. Sci. Tech. Res. 14 (1) (2020) 42–49. https://doi.org/10.12913/22998624/113425.
[53] C. Copeland, C.C. Reyes, J.L. Peck, R. Srivastava, J.M. Zuniga, Functional performance and patient satisfaction comparison between a 3D printed and a standard transradial prosthesis: a case report, Biomed. Eng. Online 21 (2022) 7, https://doi.org/10.1186/s12938-022-00977-w.
[54] J. Zuniga, K. Young, J. Peck, R. Srivastava, J. Pierce, D. Dudley, D. Salazar, J. Bergmann, Remote fitting procedures for upper limb 3D printed prostheses, Expert Rev. Med. Dev. 16 (2019) 1572506, https://doi.org/10.1080/17434440.2019.1572506.
[55] P. Borracci, R. Guachi, L. Paternò, I. Mannari, F. Napoleoni, M. Controzzi, Organizing and prioritizing user needs for upper limb prostheses, IEEE Int. Conf. Rehabil. Robot. (2025), https://doi.org/10.1109/ICORR66766.2025.11063034.
[56] P.V. Osswald, P. Obst, G.A.M. Capote, M. Friedrich, D. Rietzel, G. Witt, Failure criterion for PA 12 multi-jet fusion additive manufactured parts, Addit. Manuf. 37 (2021) 101668, https://doi.org/10.1016/j.addma.2020.101668.
[57] A. Zakręcki, J. Cieślik, A. Bazan, P. Turek, Innovative approaches to 3D printing of PA12 forearm orthoses: a comprehensive analysis of mechanical properties and production efficiency, Mater 17 (3) (2024) 663, https://doi.org/10.3390/ma17030663.
[58] L. Romanelli, C. Santus, I. Senegaglia, F. Tamburrino, M. Controzzi, A. Corrado, M. Perini, D. Kumar, R. De Biasi, M. Benedetti, Lightweight design of polymeric thin-walled components: latticization and elastic-plastic homogenization, J. Mater. Res. Technol. 36 (2025) 2977–2993, https://doi.org/10.1016/j.jmrt.2025.03.137.
[59] https://hp3dprint.eu/downloads/HPPA12Datasheet.pdf.
[60] S. Mihcin, A.M. Sahin, M. Yilmaz, A.T. Alpkaya, M. Tuna, S. Akdeniz, N.K. Can, A. Tosun, S. Sahin, Database covering the prayer movements which were not available previously, Sci. Data 10 (1) (2023) 276, https://doi.org/10.1038/s41597-023-02196-x.
[61] A. Coluccia, G. De Pasquale, Strain-based method for fatigue failure prediction of additively manufactured lattice structures, Sci. Rep. 13 (2023) 22775, https://doi.org/10.1038/s41598-023-49846-z.
[62] L. Wang, Z. Qiu, L. Tang, F. Huang, P. Wei, S. Mihcin, C. Sun, H. Zhao, L. Shi, S. Han, D. Li, A fiber-driven finite element model for predicting residual limb soft tissue deformation: applications in prosthetic socket design, Ann. Biomed. Eng. 54 (1) (2025) 211–224, https://doi.org/10.1007/s10439-025-03825-9.
[63] R.D. Biasi, L. Romanelli, C. Santus, M. Perini, F. Berto, M. Benedetti, Fatigue life prediction of multi jet fusion-manufactured polyamide12 lattice structures using the average strain energy density method, Int. J. Fatigue (2025), https://doi.org/10.1016/j.ijfatigue.2025.109452.
[64] S. Mihcin, Simultaneous validation of wearable motion capture system for lower body applications: over single plane range of motion (ROM) and gait activities, Biomed. Tech. (Biomed. Eng.) 67 (3) (2022) 185–199, https://doi.org/10.1515/bmt-2021-0429.